

# Extras from bow papers

William J. Henney, S. Jane Arthur, & Jorge A. Tarango-Yong

*Instituto de Radioastronomía y Astrofísica, Universidad Nacional Autónoma de México, Apartado Postal 3-72, 58090 Morelia, Michoacán, México*

Accepted XXX. Received YYY; in original form ZZZ

## ABSTRACT

This is material that I have taken out of the current papers. Some of it might get used in subsequent papers, especially the inertia-confined dust wave simulations and synthetic images. Also, it should inspire similar stuff but using the drag-confined magnetic dust wave models.

**Key words:** circumstellar matter – radiation: dynamics – stars: winds, outflows

## 1 TOY MODEL OF DUST WAVE WITH GAS DRAG

More realistically, a grain will also be subject to a drag force,  $f_{\text{drag}}$ , due to its relative motion with respect to gas or plasma particles. If the gas density, velocity, and sound speed are  $\rho_{\text{gas}}$ ,  $v_{\text{gas}}$ , and  $c_{s,\text{gas}}$ , then a grain with velocity  $v_d$  will experience a drag force that is directed opposite to the relative velocity,  $w = v_d - v_{\text{gas}}$ . In the supersonic limit,  $w \equiv |w| \gg c_{s,\text{gas}}$ , the magnitude of the force is

$$|f_{\text{drag}}| \approx Q_{\text{drag}} \sigma_d \rho_{\text{gas}} w^2, \quad (1)$$

where  $Q_{\text{drag}}$  is an efficiency factor (which may be smaller or greater than unity) that accounts for details such as sticking probability and the boost in cross section due to the Coulomb force when a charged grain interacts with an ionized plasma (Draine & Salpeter 1979). We neglect the back reaction of the dust on the gas motion and assume a uniform background gas flow that is perfectly coupled to the incoming dust stream at large radii. So, for the parallel stream case, we have  $v_{\text{gas}} = -v_\infty \hat{x}$  everywhere.

Considering the incoming flow on the symmetry axis, at each radius there is an asymptotic gas-grain drift speed,  $w_{\text{drift}}$ , for which the radiative and drag forces exactly cancel,  $f_{\text{drag}} = -f_{\text{rad}}$ , yielding

$$w_{\text{drift}} = \left( \frac{Q_p L}{4\pi c Q_{\text{drag}} \rho_{\text{gas}} R^2} \right)^{1/2}. \quad (2)$$

Any deviation of  $w$  from  $w_{\text{drift}}$  produces unbalanced forces that tend to restore  $w \rightarrow w_{\text{drift}}$ , although the grain inertia means that this will not happen instantaneously, so that if  $w_{\text{drift}}$  varies rapidly along a streamline, then changes in  $w$  will lag behind. We define a dimensionless coupling coefficient,  $\alpha_{\text{drag}}$ , to be the speed of the incoming stream in units of the drift velocity at the radiative turn-around radius:

$$\alpha_{\text{drag}} \equiv \frac{v_\infty}{w_{\text{drift}}(R_{**})} = \left( Q_{\text{drag}} \frac{R_{**}/a_d}{\rho_d/\rho_{\text{gas}}} \right)^{1/2}, \quad (3)$$

where we have used equation (??) and suppressed a grain-shape dependent geometric factor of order unity. If  $\alpha_{\text{drag}} \ll 1$ , then  $w_{\text{drift}} \gg v_\infty$  out to several times the turn-around radius, so the radiation field has no difficulty in effectively decoupling the grain from the gas and producing the velocity difference that is required

to turn the grain around and expel it towards the direction whence it came ( $w = 2v_\infty$ ). However, for non-zero  $\alpha_{\text{drag}}$  the  $R^{-1}$  dependence of  $w_{\text{drift}}$  (eq. (2)) means that the grain will *re-couple* to the inflowing gas stream around a radius  $\approx R_{**}/\alpha_{\text{drag}}$  and be swept back in again for another approach to the source. A further effect of increasing  $\alpha_{\text{drag}}$  is that the grain penetrates closer to the star on its initial approach, thanks to the tail wind provided by the gas flow. Both these behaviors are illustrated in Figure 1, where the inertial lag of  $w$  behind  $w_{\text{drift}}$  means that the phase space trajectory (panel b) is a spiral, which converges on the stagnation point  $(R, v) = (R_{**}/\alpha_{\text{drag}}, 0)$ . The cases  $\alpha_{\text{drag}} = 0.5$  and  $\alpha_{\text{drag}} = 2$  are shown, and it can be seen that with larger  $\alpha_{\text{drag}}$  the oscillations about the stagnation radius are significantly damped.

However, this description only applies to grains with impact parameter,  $b$ , that is exactly zero. Even a very small finite  $b$  means that  $f_{\text{rad}}$  has a component perpendicular to the axis, which pushes the grain to the side and means that, after re-coupling, its second approach is at a much larger impact parameter than its first, so it is dragged around the wings of the bow wave before it can bounce in and out more than twice. This is illustrated in Figure 2, which shows grain trajectories and the resulting dust density structure, calculated from numerical integration of equations (??) and (1) in 2-D cylindrical coordinates. Results are shown for a range of coupling parameters,  $\alpha_{\text{drag}}$ . The  $\alpha_{\text{drag}} = 0.25$  case appears qualitatively similar to the no-drag case shown in Figure ??a, except that the inner edge of the bow wave has been shifted to a smaller radius. Recoupling of the outgoing streamlines to the gas flow does occur eventually, but on length scales larger than shown in the figure. The  $\alpha_{\text{drag}} = 0.5$  case shows the oscillating trajectories discussed above for those grains that come in with a small initial impact parameter. In the  $\alpha_{\text{drag}} = 1.0$  case, the oscillating trajectories are more confined, forming a thick shell around  $R_{**}$ . In the  $\alpha_{\text{drag}} = 2.0$  case, the shell is much thinner and concentrated at the inner rim. As  $\alpha_{\text{drag}}$  increases, the oscillations are damped further so that the stagnation radius  $R_{**}/\alpha_{\text{drag}}$  becomes a good approximation to the apex radius of the density wave. All the cases illustrated are for a parallel incident stream, but a divergent stream gives qualitatively similar behavior, as shown in Appendix ???. We propose the term *dragoid* for the 3-dimensional shapes of the bow waves, found by rotating results such as Figure 2 about the symmetry axis.

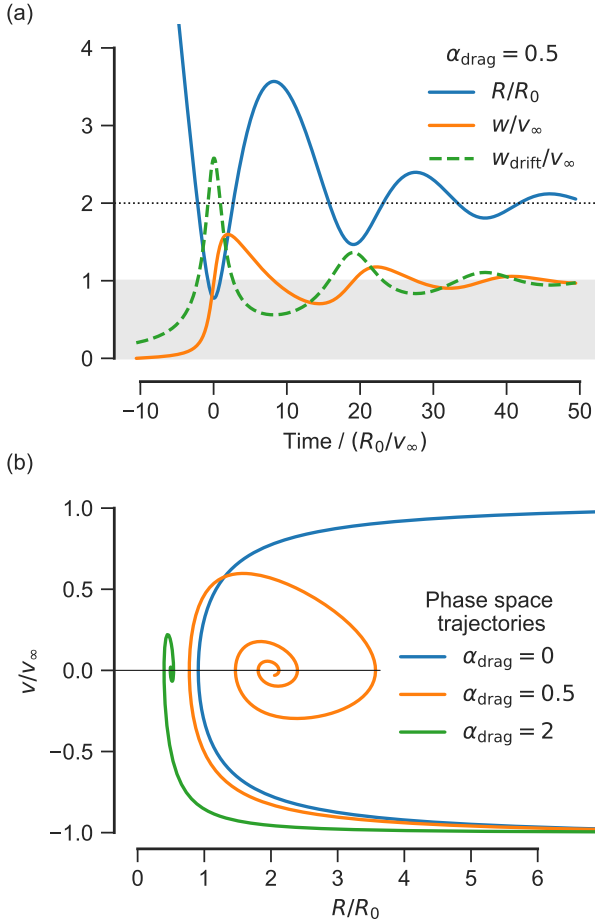


**Figure 1.** Dust-gas coupling for an on-axis (purely radial) trajectory. (a) Grain radial position,  $R/R_{**}$ , gas–grain velocity difference,  $w/v_\infty$ , and local asymptotic drift velocity,  $w_{\text{drift}}/v_\infty$ , versus time for  $\alpha_{\text{drag}} = 0.5$ . The behavior is typical of the dynamics of a damped harmonic oscillator. (b) Phase space (position, velocity) trajectories for  $\alpha_{\text{drag}} = 0, 0.5$ , and 2. All trajectories begin in the lower right corner and evolve in a clockwise direction. For  $\alpha_{\text{drag}} > 0$ , the grain spirals in on the point  $(x, u) = (\alpha_{\text{drag}}^{-1}, 0)$ .

## 2 DUST WAVE WITH MAGNETIC FIELD

*Do the analytic solution for parallel case. Discuss perp case too - see figure.*

First consider the limit of very small gyro-radius, which is the case when the Lorentz force is much larger than other forces acting on the grain. The grains will then follow tightly wound helical paths around the magnetic field lines, which can be decomposed into a circular motion of radius  $r_L$  plus the motion of the *guiding center* along the field line. The motion of the guiding center is explicitly followed by accounting for the components parallel to the field lines of the radiative and drag forces, whereas forces perpendicular to the field lines, which would only effect the circular motion are ignored in the first instance (but see § XXX below).

### 2.1 Resolved Larmor radius

## 3 APPLICABILITY OF THE DUST WAVE MODELS

The apex turn-around radius,  $R_{**}$ , of the bow wave depends on the grain properties via the combination  $\sigma_d Q_p m_d$ . For grains of size  $a_d$  and internal density  $\rho_d$ , we have  $\sigma_d/m_d \approx (a_d \rho_d)^{-1}$ . For radiation with wavelength smaller than the grain size,  $\lambda < a_d$ , the efficiency is  $Q_p \sim 1$ , whereas for  $\lambda > a_d$  it is  $Q_p \sim a_d/\lambda$ . Therefore, we would expect  $R_{**}$  to be almost independent of grain size for small grains, but to vary as  $R_{**} \propto a_d^{-1}$  for large grains, where small/large is relative to the peak wavelength of the radiation source. In principle, a polydisperse population of grains could produce a blurring of the observed bow wave, but only if large grains contribute significantly to the dust emission.

Variation of  $\alpha_{\text{drag}}$  with grain size, charged grains.

Lorentz force, Larmor radius

Back-reaction on gas,  $\alpha_{\text{drag}} \rightarrow \infty$ , recovery of drag-free result for  $R_0$  but with increased effective grain mass.

## 4 APPARENT SHAPES OF PROJECTED DRAGODIDS

## 5 SHAPE AND STRUCTURE OF BOW WAVES

## REFERENCES

Draine B. T., Salpeter E. E., 1979, ApJ, 231, 77

Tarango Yong J. A., Henney W. J., 2018, MNRAS, in preparation

This paper has been typeset from a TeX/LaTeX file prepared by the author.

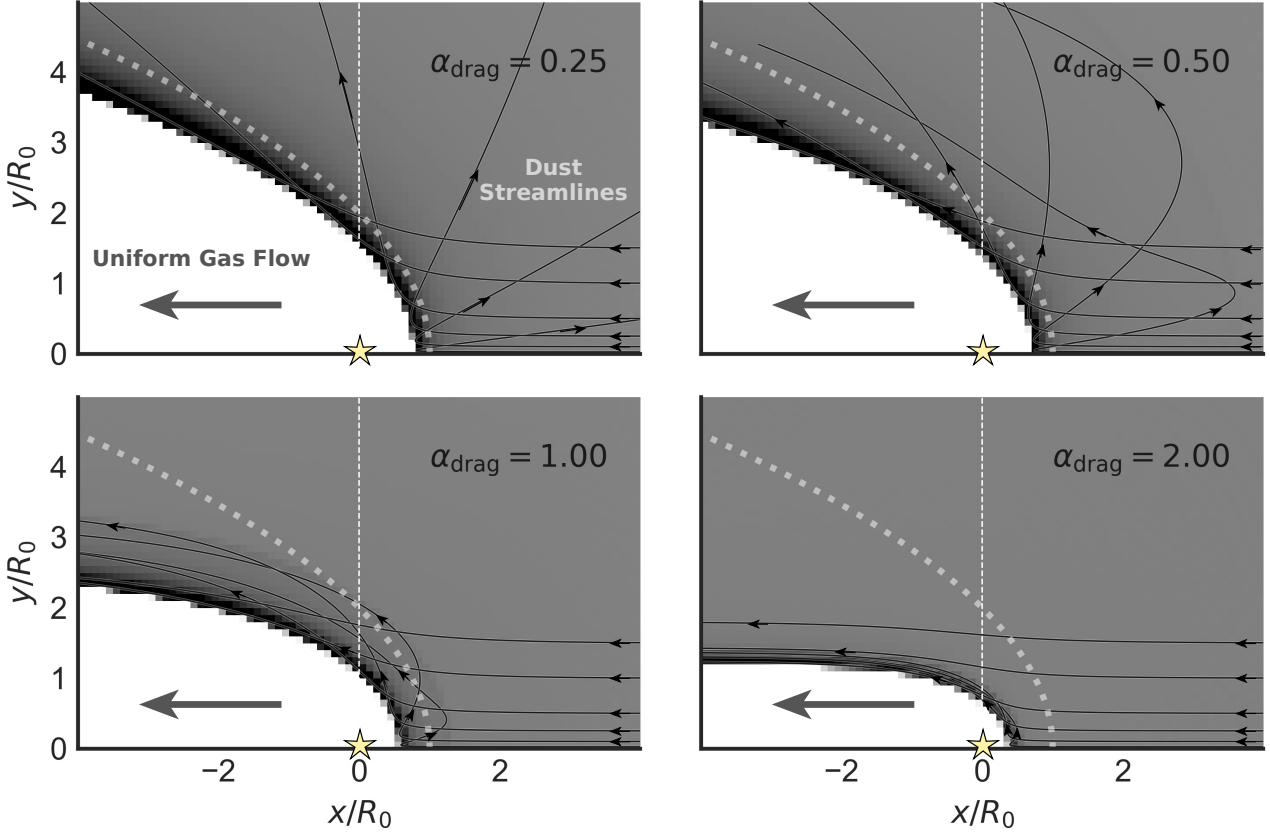


**Figure 2.** Dust grain trajectories under influence of gas drag in addition to a repulsive central radiative force. The dust streamlines are shown as black lines with arrows and the dust density as a linear gray scale, with maximum (black) of twice the ambient dust density. Results are shown for four values of the drag parameter (see text):  $\alpha_{\text{drag}} = 0.25, 0.5, 1.0,$  and  $2.0.$  The shape of the bow wave for the drag-free case (Fig. ??) is shown by the thick dotted line. Faint patterns visible in the density away from the bow wave are numerical aliasing artefacts caused by sparse sampling of the streamlines in the low density regions.

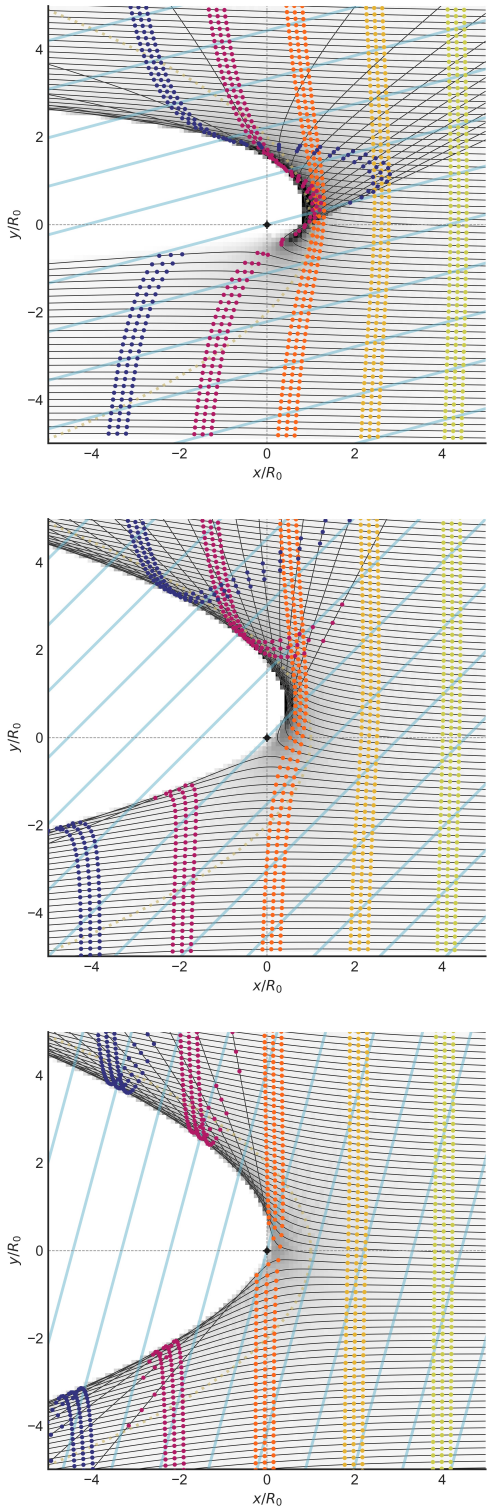


**Figure 3.** Grain trajectories for magnetised dust waves in the limit of no gas drag and small gyro-radius.

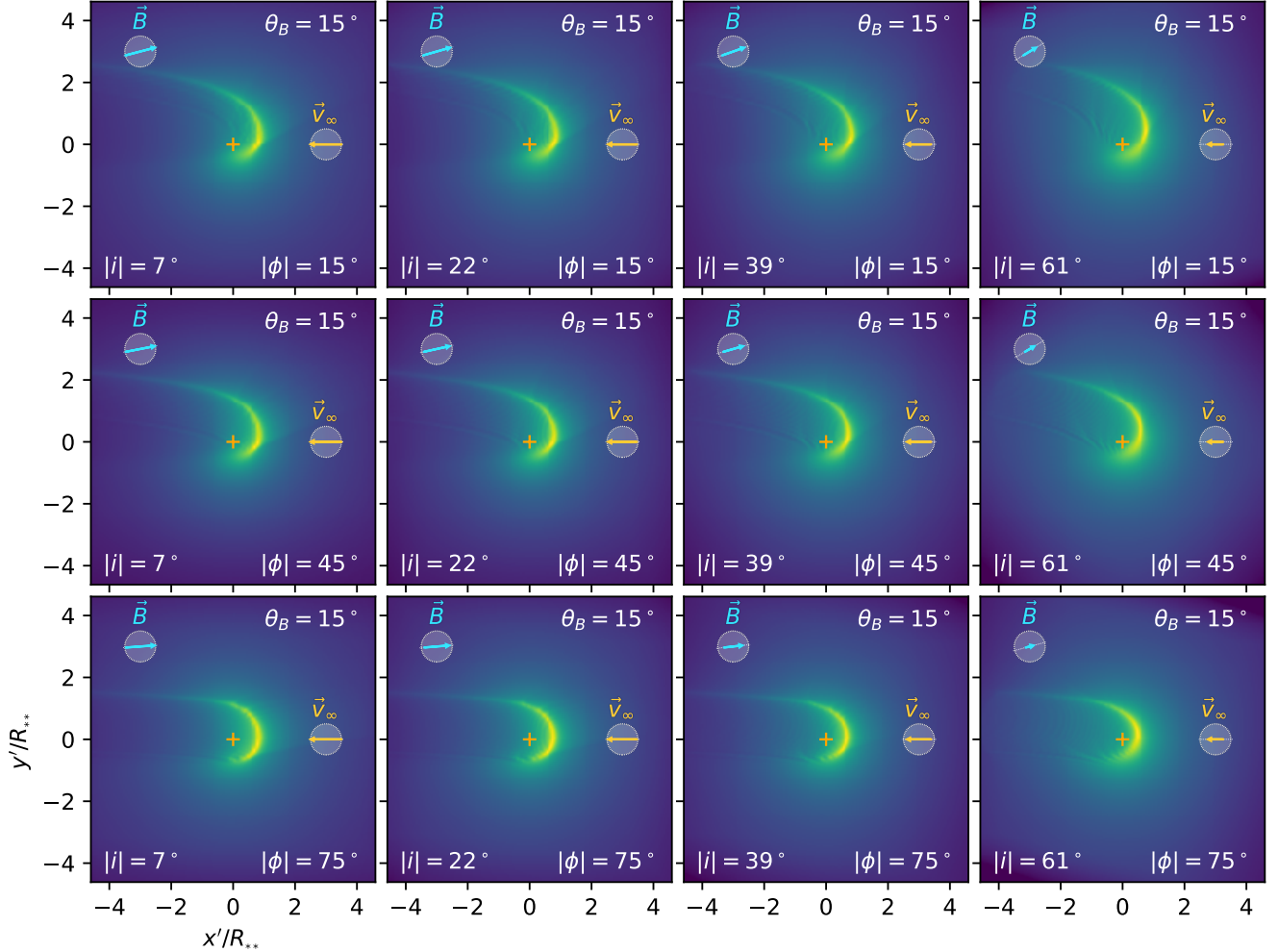
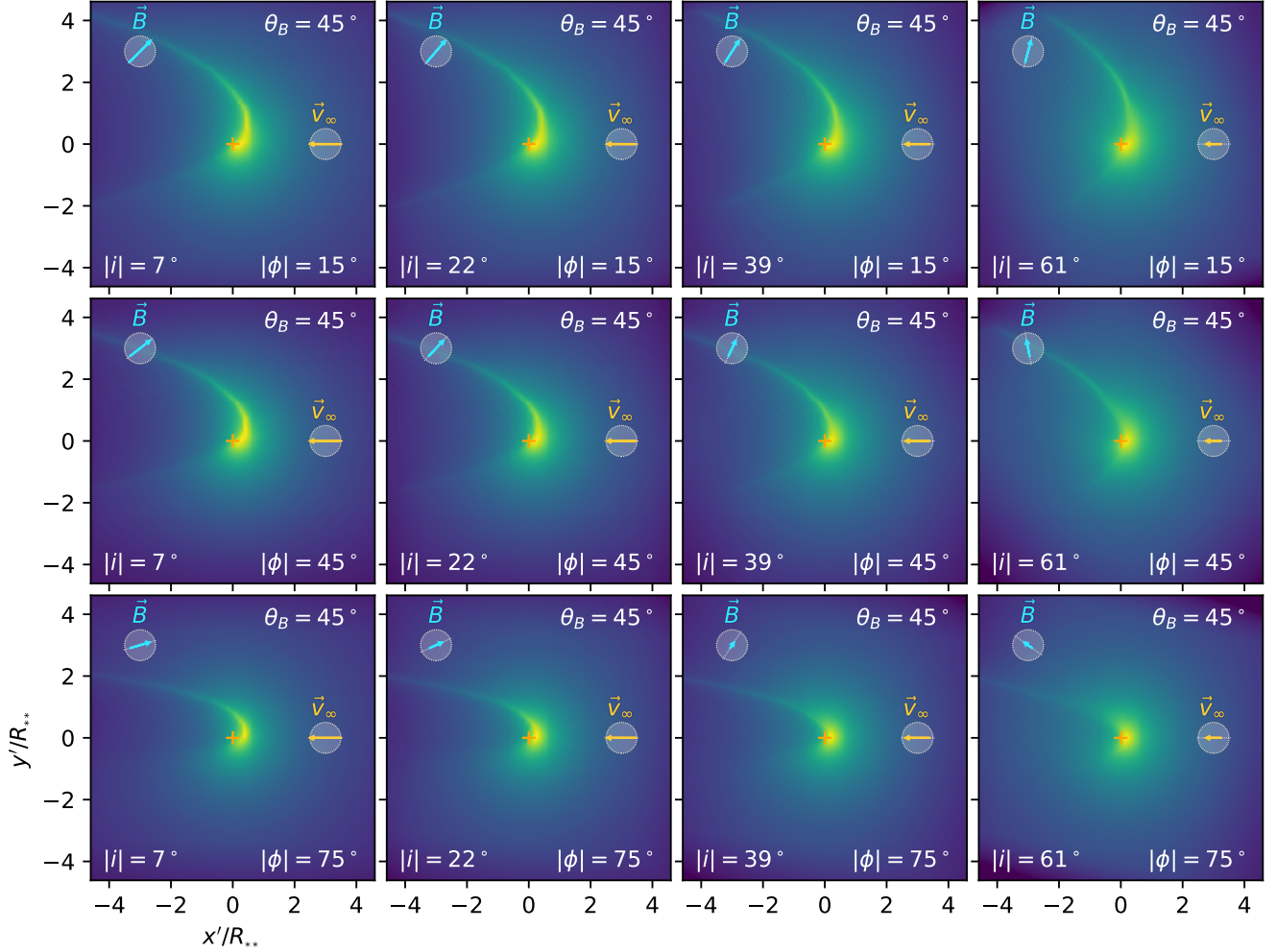


Figure 4. xxx

**Figure 5.** xxx

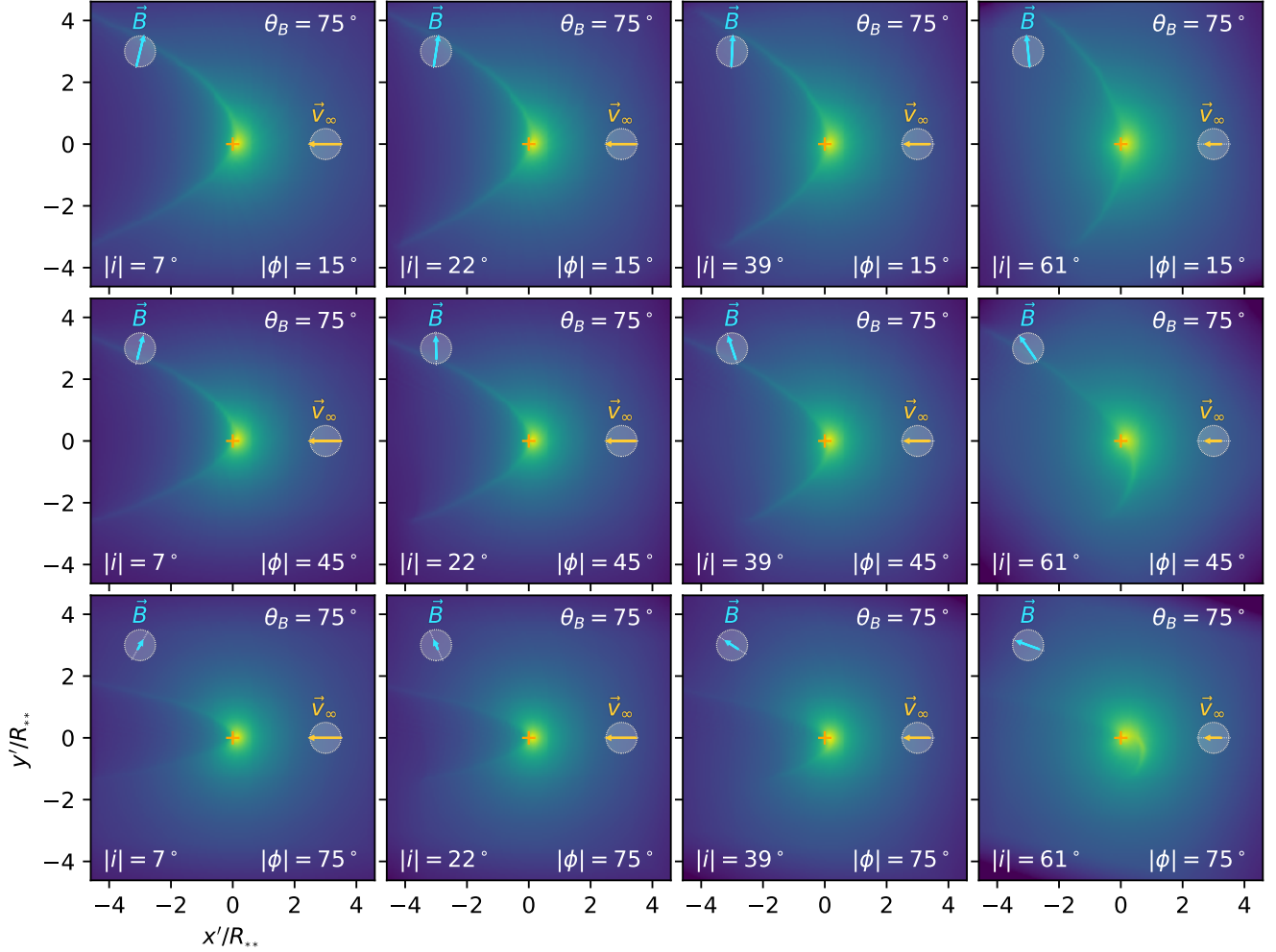
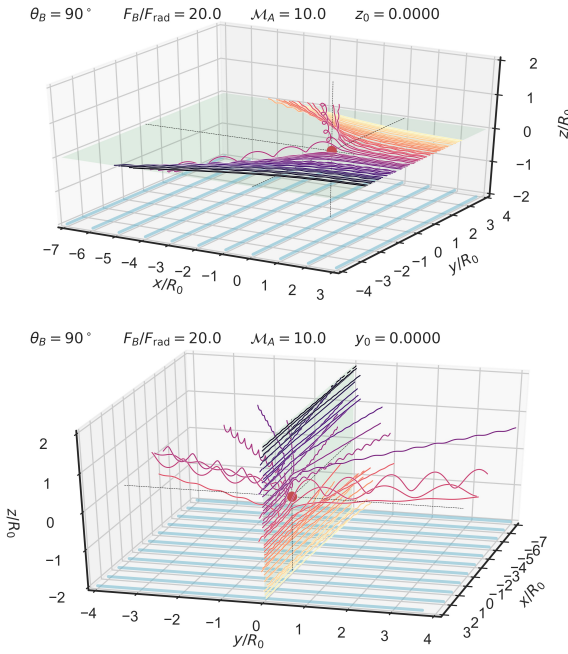
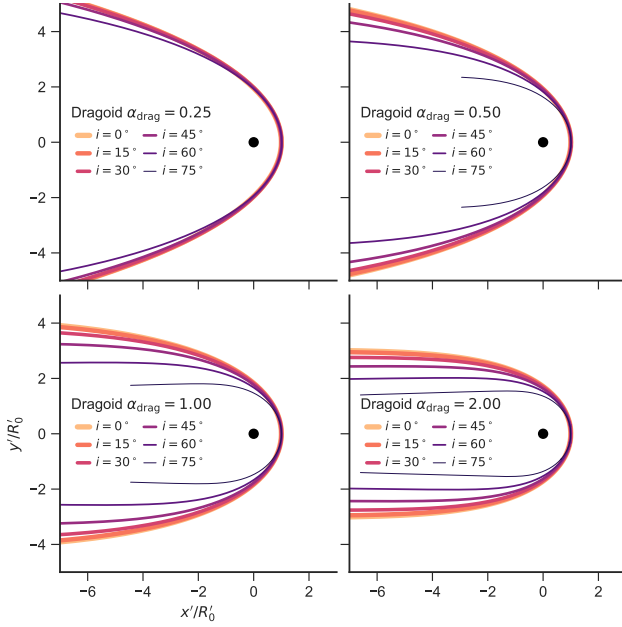


Figure 6. xxx



**Figure 7.** Streamlines in three dimensions of resolved gyro-radius



**Figure 8.** Apparent bow shapes in the plane of the sky for parallel-stream dragoids as a function of inclination angle. Drag coefficient,  $\alpha_{\text{drag}}$  increases from top-left to bottom-right. Inclination  $|i|$  is shown in  $15^\circ$  increments, indicated by line color and thickness (see key).

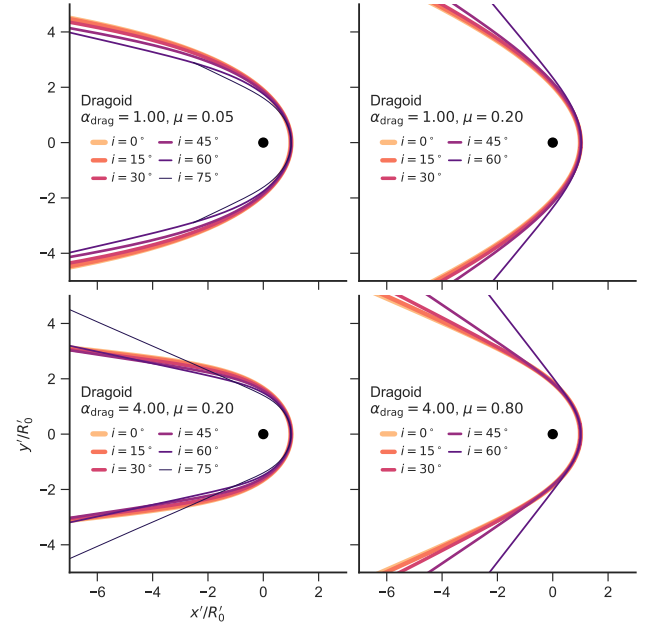


**Figure 9.** As Fig. 8 but for divergent stream dragoids. Drag coefficient increases from top to bottom, while degree of divergence increases from left to right.

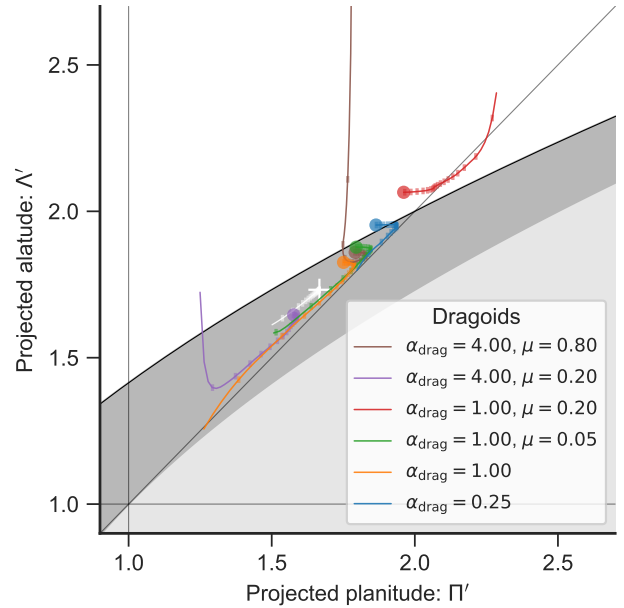


**Figure 10.** Apparent projected shapes of dragoids in the  $\Pi'$ – $\Lambda'$  plane. Colored symbols indicate the  $|i| = 0$  position for selected models (see key). Thin lines show the inclination-dependent tracks of each model, with tick marks along each track for 20 equal-spaced values of  $|\sin i|$ . Gray shaded regions are as in Fig. 11a of Paper I. The wilkinoid track is shown in white.